Physiological Measurement

IPEM
Institute of Physics and Engineering in Medicine

PAPER • **OPEN ACCESS**

Evaluation of five methods for the interpolation of bad leads in the solution of the inverse electrocardiography problem

To cite this article: Y Serinagaoglu Dogrusoz *et al* 2024 *Physiol. Meas.* **45** 095012

View the article online for updates and enhancements.

You may also like

- Corrigendum: Highly comparative time series analysis of oxygen saturation and heart rate to predict respiratory outcomes in extremely preterm infants (2024 *Physiol. Meas.* 45 055025)
Jiaxing Qiu, Juliann M Di Fiore, Narayanan Krishnamurthi et al.
- Highly comparative time series analysis of oxygen saturation and heart rate to predict respiratory outcomes in extremely preterm infants
Jiaxing Qiu, Juliann M Di Fiore, Narayanan Krishnamurthi et al.
- Cycle-frequency content EEG analysis improves the assessment of respiratory-related cortical activity
Xavier Navarro-Sune, Mathieu Raux, Anna L Hudson et al.

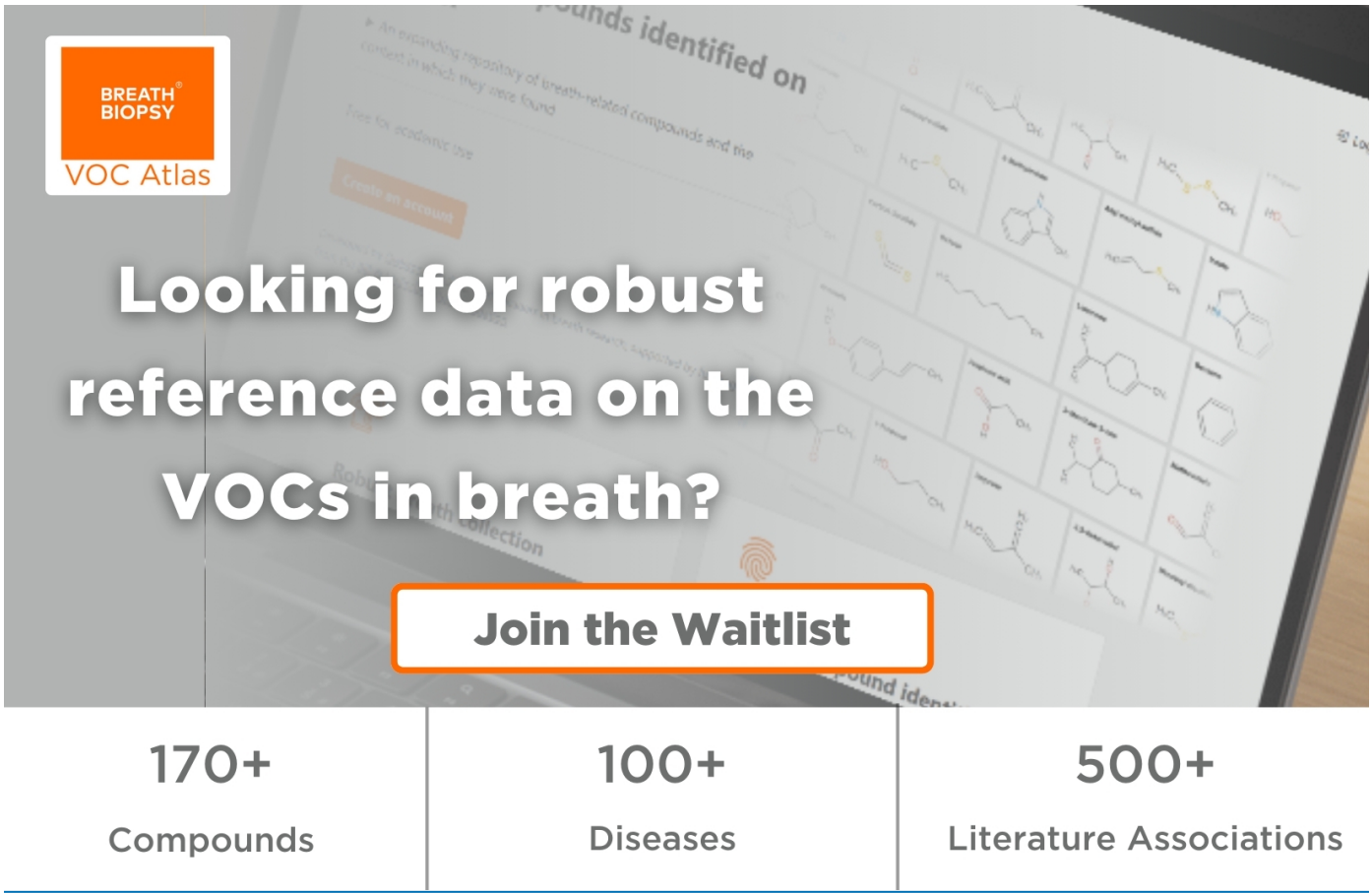

This content was downloaded from IP address 144.122.7.71 on 11/11/2024 at 12:50

IOP Publishing Physiol. Meas. 45 (2024) 095012 https://doi.org/10.1088/1361-6579/ad74d6

Physiological Measurement

IPEM Institute of Physics and Engineering in Medicine

CrossMark

OPEN ACCESS

RECEIVED
6 March 2024

REVISED
5 July 2024

ACCEPTED FOR PUBLICATION
28 August 2024

PUBLISHED
24 September 2024

Original Content from this work may be used under the terms of the Creative Commons Attribution 4.0 licence.

Any further distribution of this work must maintain attribution to the author(s) and the title of the work, journal citation and DOI.

PAPER

Evaluation of five methods for the interpolation of bad leads in the solution of the inverse electrocardiography problem

Y Serinagaoglu Dogrusoz[1,*], L R Bear[2,3,4], J A Bergquist[5,6,7], A S Rababah[9], W Good[10], J Stoks[11], J Svehlikova[12], E van Dam[13], D H Brooks[14] and R S MacLeod[5,6,7,8]

[1] Middle East Technical University, Department of Electrical and Electronics Engineering, Ankara, Turkey
[2] IHU-LIRYC, Fondation Bordeaux Université, Pessac, France
[3] Univ. Bordeaux, CRCTB, U1045 Bordeaux, France
[4] INSERM, Centre de recherche Cardio-Thoracique de Bordeaux, U1045 Bordeaux, France
[5] Scientific Computing and Imaging (SCI) Institute, University of Utah, Salt Lake City, UT, United States of America
[6] Nora Eccles Harrison Cardiovascular Research and Training Institute (CVRTI), University of Utah, Salt Lake City, UT, United States of America
[7] Department of Biomedical Engineering, University of Utah, Salt Lake City, UT, United States of America
[8] School of Medicine, University of Utah, Salt Lake City, UT, United States of America
[9] Jordanian Royal Medical Services, Amman, Jordan
[10] Acutus Medical, Carlsbad, CA, United States of America
[11] Cardiovascular Research Institute Maastricht, Maastricht University, Maastricht, The Netherlands
[12] Slovak Academy of Sciences, Institute of Measurement Science, Bratislava, Slovakia
[13] Peacs, Nieuwerbrug, The Netherlands
[14] Department of Electrical and Computer Engineering, Northeastern University, Boston, MA, United States of America
[*] Author to whom any correspondence should be addressed.

E-mail: yserin@metu.edu.tr

Keywords: Inverse electrocardiography, electrocardiographic imaging, body surface potential measurements, interpolation

Supplementary material for this article is available online

Abstract

Objective. This study aims to assess the sensitivity of epicardial potential-based electrocar diographic imaging (ECGI) to the removal or interpolation of bad leads. *Approach.* We utilized experimental data from two distinct centers. Langendorff-perfused pig ($n = 2$) and dog ($n = 2$) hearts were suspended in a human torso-shaped tank and paced from the ventricles. Six different bad lead configurations were designed based on clinical experience. Five interpolation methods were applied to estimate the missing data. Zero-order Tikhonov regularization was used to solve the inverse problem for complete data, data with removed bad leads, and interpolated data. We assessed the quality of interpolated ECG signals and ECGI reconstructions using several metrics, comparing the performance of interpolation methods and the impact of bad lead removal versus interpolation on ECGI. *Main results.* The performance of ECG interpolation strongly correlated with ECGI reconstruction. The hybrid method exhibited the best performance among interpolation techniques, followed closely by the inverse-forward and Kriging methods. Bad leads located over high amplitude/high gradient areas on the torso significantly impacted ECGI reconstructions, even with minor interpolation errors. The choice between removing or interpolating bad leads depends on the location of missing leads and confidence in interpolation performance. If uncertainty exists, removing bad leads is the safer option, particularly when they are positioned in high amplitude/high gradient regions. In instances where interpolation is necessary, the inverse-forward and Kriging methods, which do not require training, are recommended. *Significance.* This study represents the first comprehensive evaluation of the advantages and drawbacks of interpolating versus removing bad leads in the context of ECGI, providing valuable insights into ECGI performance.

© 2024 The Author(s). Published on behalf of Institute of Physics and Engineering in Medicine by IOP Publishing Ltd

1. Introduction

Electrocardiographic imaging (ECGI) has emerged as a powerful tool for non-invasive cardiac mapping, offering insights into cardiac electrical activity and enabling valuable pre-procedure diagnosis and guidance for cardiac ablation procedures (Cluitmans *et al* 2015, Cluitmans 2018, Bergquist *et al* 2021). However, the presence of bad leads (BLs)-leads with incomplete or erroneous data-can compromise the accuracy of ECGI. This study explores the impact of handling BLs by either removing them or employing interpolation methods. Through the evaluation of ECG interpolation and ECGI reconstruction performances, we provide a comprehensive analysis of the benefits and risks associated with these approaches, shedding light on their significance in the field of ECGI.

In ECGI, BSP measurements are recorded by multi-electrode acquisition systems. The number of electrodes in these systems normally ranges from 32 to 219, covering the front and back of the torso (Hoekema *et al* 1999). However, when the ECGI solutions are applied in the electrophysiology (EP) laboratory, the safety of the patient is rightly placed above the need for a large number of good contact signals for ECGI reconstructions. This has led to the acquisition of highly valuable data sets in patients in which large portions of the torso are missing electrical data due to the simultaneous placement of CARTO reference electrodes and defibrillator patches (Nademanee *et al* 2019, Stoks *et al* 2023). There is a lack of literature and consensus on how to handle these missing/bad BSP leads in the ECGI reconstructions, which is one of the major challenges in adopting ECGI into real-time clinical applications.

Researchers have explored methods to optimize the selection of BSP leads, reducing the number of leads while maintaining diagnostic accuracy (Barr *et al* 1971, Lux *et al* 1978, 1979, Finlay *et al* 2006, 2008b, Gharbalchi No *et al* 2020, Onak *et al* 2022), or interpolating missing leads (Barr *et al* 1971, Lux *et al* 1978, 1979, Castells *et al* 2007, Donnelly *et al* 2008). Such methods have been implemented to replace missing/broken leads for ECGI reconstructions (Burnes *et al* 1998, Sapp *et al* 2012).

Burnes *et al* proposed the inverse-forward (IF) method, a field-compatible approach for interpolating missing leads (1998). They compared the ECGI performance of the IF method with linear and Laplacian interpolation, ultimately favoring the IF method for its superior accuracy, particularly for interpolating larger regions. Bear *et al* compared the ECGI performance of removing the BLs versus reconstructing the missing leads using linear interpolation (2015). Their findings demonstrated that the removal of BLs led to more accurate ECGI reconstructions (Bear *et al* 2015). Ghodrati *et al* evaluated interpolating missing leads by Laplacian interpolation and Bayesian estimation in contrast to lead removal (2007). They highlighted that in the absence of prior information, simply dropping the missing leads outperformed Laplacian interpolation. In Rababah *et al* (2018), Laplacian interpolation outperformed the principle component analysis (PCA)-based method in estimating the missing data in BSPs. In a follow-up study, a hybrid method combining both interpolation methods led to a more accurate estimation of the missing leads when compared to employing each method individually (Rababah *et al* 2019). Finally, Rababah *et al* explored the impact of interpolating or eliminating low-amplitude ECG leads on ECGI performance and determined that interpolation has the potential to enhance reconstruction accuracy (2019, 2021). However, these studies evaluated only limited aspects of handling missing or BLs. Moreover, the conflicting results seen in these different studies demonstrate the need for a more comprehensive investigation to determine the optimal approach for ECGI. This study aims to fill this gap in the literature by presenting a thorough analysis and comparison of various interpolation methods and the removal of BLs using data from two centers, encompassing a diverse dataset.

In a preliminary study, our group investigated several interpolation methods and discussed their potential use instead of lead removal for a single dataset (Dogrusoz *et al* 2019). In this expanded research, we conduct a thorough evaluation of interpolation performance using data from different centers, including Langendorff-perfused pig and dog hearts. We generate six distinct configurations of BLs and employ five interpolation methods to rectify the missing data. We solve the inverse problem by the zero-order Tikhonov regularization, employing three distinct datasets: the complete data, data after lead removal, and the interpolated data. We assess the accuracy of interpolated ECG signals and the resultant ECGI reconstructions, specifically focusing on interpolation accuracy and the consequences of lead removal versus interpolation for ECGI performance.

2. Methods

2.1. Experimental data sets

This study utilized four experimental data sets from two distinct torso tank setups: one at IHU-LIRYC (Bordeaux, France) and the other at the CRVTI/SCI Institutes (Salt Lake City, Utah). These same data sets

Table 1. Number (#) and percentage (%) of removed leads for all bad lead configurations in all datasets.

	Bord-1		Bord-2		Utah-1&2	
	#	%	#	%	#	%
BL1	15	11.7	20	15.6	19	9.9
BL2	12	9.4	17	13.3	19	9.9
BL3	13	10.2	18	14.1	21	10.9
BL4	15	11.7	20	15.6	13	6.8
BL5	17	13.3	20	15.6	38	19.8
BL6	57	44.5	60	46.9	77	40.1

were previously employed in Bear *et al* (2021), which offers a more detailed account. Here is a brief overview of these setups.

2.1.1. Bordeaux setup

Two data sets from IHU-LIRYC involved Langendorff-perfused pig hearts suspended in a human-shaped torso-tank (Bear *et al* 2018). These experimental procedures were approved by the Directive 2010/63/EU of the European Parliament on the protection of animals used for scientific purposes and the local ethical committee. Simultaneous recordings of epicardial electrograms were made using a 108-electrode epicardial array (inter-electrode spacing of 9.9 $\pm$ 2.2 mm), along with ECGs from 128 electrodes (inter-electrode spacing of 66 $\pm$ 24 mm) embedded in the tank surface. These recordings were made during right ventricular (RV) pacing with a 2048 Hz sampling rate (BioSemi, the Netherlands). Afterward, 3D fluoroscopy (Artis, Siemens) was used to determine the positions of the electrodes in relation to the tank.

2.1.2. Utah setup

Two data sets from the CRVTI/SCI Institutes employed Langendorff-perfused canine hearts, also suspended in a human-shaped torso-tank (Shome and MacLeod 2007, Bergquist *et al* 2021). Arterial blood was supplied from a second canine under deep anesthesia. These experimental procedures were approved by the Institutional Animal Care and Use Committee of the University of Utah and conformed to the Guide for the Care and Use of Laboratory Animals protocol number 17-04 016 approved on 05/17/2017. Recordings included epicardial electrograms from a 247-electrode epicardial sock (inter-electrode spacing of 6.5$\pm$1.3 mm) and ECGs from 192 electrodes (inter-electrode spacing of 40.2$\pm$16.8 mm) embedded in the tank surface. These recordings were made during RV pacing at a 1000 Hz sampling rate, utilizing a custom acquisition and multiplexing system. After the experiments, a three-dimensional mechanical digitizer (Microscribe from Immersion Corp.) was used to locate landmarks on the tank and electrode array, providing reference points for sock geometry registration within the torso tank (Bergquist *et al* 2019). Signal processing was carried out using PFEIFER, an open-source software tool designed for processing time series data from electrocardiographic experiments (Rodenhauser *et al* 2018).

All ECG signals from both systems were initially filtered using a bandpass filter (0.5–150 Hz cut-off frequencies), and a notch filter at the line frequency.

2.2. BL configurations

In this study, we created six BL configurations to simulate realistic clinical scenarios. These scenarios included two defibrillation patch setups (BL1 and BL2), the presence of CARTO reference electrodes (BL3), and missing electrodes on the shoulders (BL4) and torso sides (BL5). BL6 represents a worst-case scenario, combining all configurations. All BL setups incorporated tank signals that were either absent or of suboptimal quality (approximately 3$\pm$2 channels), and these problematic leads were excluded from the inverse calculations when using the complete lead set (FULL). For detailed statistics on the number and percentage of removed leads in the various datasets, please refer to table 1. Sample BL configurations are presented in figure 1 for the Bordeaux tank.

2.3. Interpolation methods

We used five common interpolation methods to replace the BLs, chosen for their widespread use in ECG and EGM interpolation across international research centers:

Laplacian interpolation (LAP) (Oostendorp *et al* 1989): this method implements an approximation of the surface Laplacian operator as the interpolation kernel which minimizes the Laplacian over the torso surface.

Inverse distance square interpolation (IDS) (Shepard 1968): here, the missing lead is estimated as the weighted sum of the available leads, with weights equal to the inverse of the square of the Euclidian distance between the target and the available leads.

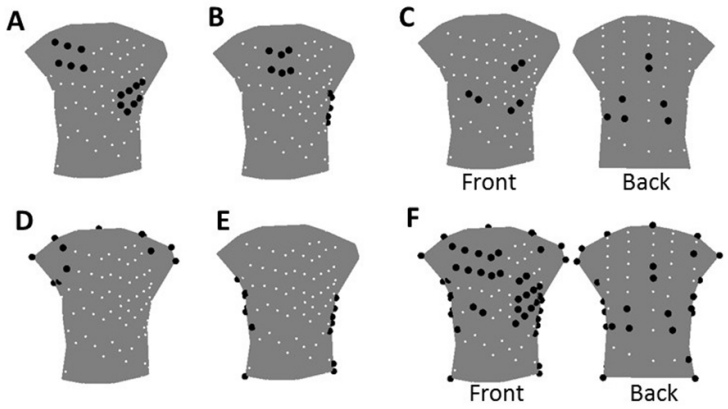

Figure 1. All BL configurations for the Bordeaux tank. Black dots represent the leads removed (i.e. bad leads) out of the full set (white dots). (A) BL1, front, (B) BL2, front, (C) BL3, front and back, (D) BL4, front, (E) BL5, front, (F) BL6 (combination of all BLs), front and back.

Kriging method (KRI) (Cressie 1990, van Beers and Kleijnen 2003): this method estimates missing ECG leads through linear combinations of available BSP data, considering spatial proximity. It aims to provide the best linear unbiased estimate, optimizing estimation by accounting for spatial correlation.

IF method (Burnes *et al* 1998): this method is a modification of the method of fundamental solutions (MFS) for ECG inverse problems (Wang and Rudy 2006). It inversely reconstructs signals on an arbitrary interior surface from available BSP data and then employs them in a forward model to compute missing ECG leads.

A hybrid method (HYB) (Rababah *et al* 2019): this method combines Laplacian and PCA interpolation methods. At each missed electrode, this method exploits the first beat of the ECG recordings and the Laplacian interpolation to estimate the ECG recordings of the following beats.

2.4. Forward and Inverse problems

Torso measurements ($\mathbf{y}_k \in \mathbb{R}^M$) can be expressed in terms of the EGMs ($\mathbf{x}_k \in \mathbb{R}^N$) as:

$$\mathbf{y}_k = \mathbf{A}\mathbf{x}_k + \mathbf{n}_k,\ k = 1, 2, \ldots, T \tag{1}$$

where k is the time instant, $\mathbf{n}_k \in \mathbb{R}^M$ models the measurement noise, and $\mathbf{A} \in \mathbb{R}^{M\times N}$ is the forward transfer matrix, which is computed using the boundary element method (BEM) for a homogeneous torso (Barr *et al* 1977), as detailed in Bear *et al* (2021).

We chose the zero-order Tikhonov regularization (Tikhonov and Arsenin 1977) due to its widespread use in the ECGI applications by major research centers to enhance the relevance and applicability of our findings to clinical settings, where standardized methods are crucial for consistency and reliability (Sapp *et al* 2012, Cluitmans *et al* 2017, Wang *et al* 2018, Bear *et al* 2019, Duchateau *et al* 2019, Molero *et al* 2023). Omitting the time index in equation (1) for simplicity, the solution can be expressed as:

$$\hat{\mathbf{x}} = \arg\min_{\mathbf{x}} \left\{ \|\mathbf{A}\mathbf{x} - \mathbf{y}\|_2^2 + \lambda^2 \|\mathbf{x}\|_2^2 \right\} \tag{2}$$

where λ is the regularization parameter. Initially, a different $\lambda(k)$ value was determined at each time instant k using the L-curve method (Hansen and Johnston 2001). Then, the median of these $\lambda(k)$ values over time were computed and defined as the final λ value for all time instants.

The inverse problem was addressed in three distinct scenarios: (1) using all measured BSPs except for the identified 'true' BLs (FULL), (2) employing the row deletion method proposed in Ghodrati *et al* (2007) to remove BLs and exclude them from inverse computations (RMV), and (3) substituting the BLs with interpolated signals.

2.5. Evaluation metrics

Five interpolation methods were applied to reconstruct the missing leads in six BL-configurations. Considering FULL (same for all BL) and RMV reconstructions, we obtained a total of 37 different EGM reconstructions for each data set (36 interpolation/RMV + FULL). The various data sets included from 13 to

31 beats. Since the smallest data set (Utah-2) consisted of 13 paced beats, we utilized only the initial 13 beats from the remaining datasets for uniformity.

Interpolation methods were evaluated for their accuracy in reconstructing both the ECGs at the specified BLs and the corresponding ECGI reconstruction of cardiac potentials.

2.5.1. ECG interpolation

The morphology of the interpolated ECGs was compared to the corresponding measured ECG leads using Pearson's correlation (CC). The error in the interpolated leads with respect to the measured leads was evaluated using the relative error (RE) metric. Both metrics were computed over the QRS region.

2.5.2. ECGI reconstruction

The morphology of the reconstructed EGMs in each lead was evaluated using the temporal CC compared to the sock data. The errors in these reconstructions were compared using the RE metric. The fidelity of the reconstructed isopotential maps at each time instant was evaluated using the spatial CC.

2.5.3. Activation time (AT) reconstruction and localization error (LE)

ATs of the sock electrodes were defined as the time at which the derivative (dV/dt) is minimum. While this simple method was sufficiently accurate for the measured EGMs, it lacked accuracy in the reconstructions. Thus we considered two spatiotemporal (ST) AT estimation methods. Both methods start by computing the temporal-only ATs using the standard minimum derivative approach. The first method is called the ST smoothing method, in which spatial smoothing is applied to the temporal AT estimates over the heart surface using a regularization operator (Erem *et al* 2014). The second method is the spatially coherent (SC) method proposed in Duchateau *et al* (2017). This method utilizes another ST approach that combines estimated time delays between neighboring electrograms with the standard temporal-only AT estimates.

Ground truth and reconstructed ATs were compared using Pearson's CC and the mean absolute error (MAE, ms). The pacing site was defined as the node with the earliest AT. The LE (mm) was calculated as the Euclidean distance between the sock (ground truth) and ECGI pacing sites.

2.5.4. Statistical tests

Statistical analysis of the ECG and ECGI metrics corresponding to different interpolation methods was conducted using the Wilcoxon rank sum test ($p < 0.05$ defined as significant) with Bonferroni adjustment.

Our comprehensive analysis involved four datasets with 13 beats each, six BL configurations, five interpolation methods, and various ECG and ECGI metrics. To summarize these results, we proposed a ranking system based on statistical comparisons. For the interpolated ECG comparisons, for each data set, each BL configuration, each interpolation method, and each beat, median values of the temporal CC and RE were calculated over all interpolated leads. Similarly, for ECGI and AT evaluations, we obtained median or mean values of metrics for each reconstruction over all leads or time instances. These computations resulted in mean or median value vectors of length equal to the number of beats.

For each ECG and ECGI metric, dataset, and BL configuration, we constructed comparison tables from the statistical tests. These tables, as shown in the top panels of figures 2 and 3, facilitated method comparisons. A '1' indicated that the method in the row significantly increased the metric compared to the method in the column, '-1' signified the opposite, and '0' meant no significant difference.

We obtained similar tables for each dataset and BL configuration. Interpolation methods were ranked based on how often they significantly increased or decreased the metric, with respect to (a) each BL configuration across all datasets (blue), (b) each dataset across all BL configurations (green), and (c) overall performance across all datasets and BL configurations (red) as depicted in the bottom panels of figures 2 and 3.

The boxplot distributions of all metrics and the ranking tables for each metric are included in the supplementary document. The results of these rankings are presented and discussed in sections 3.3.1 and 3.3.2.

3. Results

3.1. Evaluation of the interpolated ECGs

We obtained boxplot distributions of median temporal CC (medCC-ECG) and median temporal RE (medRE-ECG) for all BL configurations and all data sets. All plots are available in the supplementary document.

Almost all medCC-ECG values were above 0.98, with the exception of IDS in a few cases ($0.93 - 0.96$) and LAP in Utah-1, BL1 (0.95), demonstrating the successful recovery of ECG morphologies by the

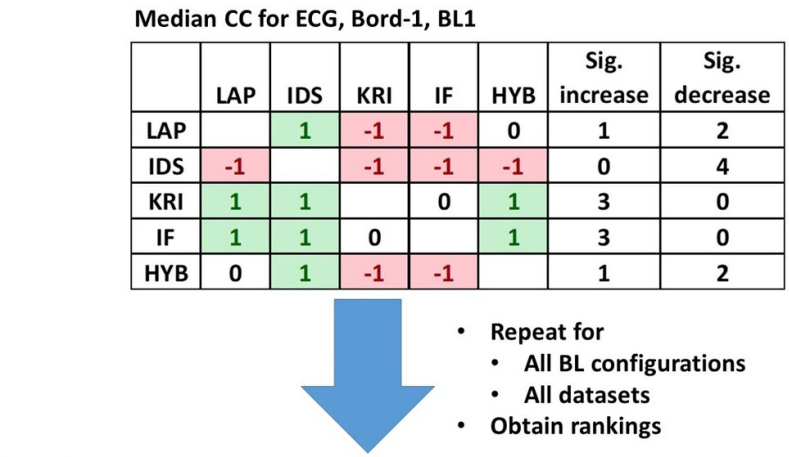

	LAP	IDS	KRI	IF	HYB	Sig. increase	Sig. decrease
LAP		1	-1	-1	0	1	2
IDS	-1		-1	-1	-1	0	4
KRI	1	1		0	1	3	0
IF	1	1	0		1	3	0
HYB	0	1	-1	-1		1	2

	BL1	BL2	BL3	BL4	BL5	BL6	Bord-1	Bord-2	Utah-1	Utah-2	Overall
LAP	4	4	4	2	3	4	3	2	4	4	4
IDS	5	5	5	5	5	5	5	5	5	5	5
KRI	3	3	1	4	2	3	1	2	2	3	2
IF	1	1	3	3	4	1	1	3	3	1	3
HYB	1	1	1	1	1	1	4	1	1	1	1

Figure 2. Illustration of ranking steps for comparing different interpolation methods for reconstructing the bad lead ECG signals. A detailed description for constructing these tables is presented in section 2.5. The top panel shows the median temporal CC comparison table for Bord-1, BL1. The bottom panel displays the combined rankings of the methods for all data sets and BL configurations, based on the number of times a method significantly increased or decreased the given metric.

interpolation methods. IDS had the lowest CC values for most data sets and for most BL configurations. IF, KRI, and the HYB were the best methods, showing similar accuracy, and the order of preference depending on both the data set and the BL configuration. Though the LAP method is often among the best methods, it performed the poorest for Utah-1, BL1, with a reduction of up to 6.2% in CC compared to the other methods including IDS.

The medRE-ECG values were mostly below 0.30, with some values between $0.30-0.50$. Again, the worst values were attained by IDS (as high as 0.73 in Bord-2 BL3; 0.40 for Bord-1 and 0.35 for Utah-2 in BL6). Despite medCC-ECG values greater than 0.93, IDS exhibited higher reconstruction errors, indicating that the QRS amplitudes cannot be recovered appropriately. The other interpolation methods showed variable performances but HYB had the lowest error except in Bord-1, BL1, with KRI a close second for most data sets and BL configurations (poor performance in Bord-1, BL1, BL5, and BL6; Bord-2, BL3; Utah-1, BL4). IF and LAP seem very dependent on the data set and BL configuration, sometimes performing as well as KRI/HYB but other times inaccurately. LAP did not work well for nearly every BL configuration for Utah-1, potentially demonstrating a stronger dependence on cardiac sequence than the position of BLs.

3.2. Evaluation of the inverse reconstructions

Boxplot distributions of all ECGI and AT metrics (median temporal CC (medCC-EGM); mean temporal CC (meanCC-EGM); median temporal RE (medRE-EGM); median spatial CC (medspatCC-EGM); CC of ATs (CC-AT); MAE in AT values (MAE-AT); LE) for all BL configurations and all data sets are similarly available in the supplementary document. Some noteworthy results are presented below.

3.2.1. ECGI performance of the interpolation methods

The medCC-EGM values were within a range of $0.63-0.75$ except in Bord-1, which were lower in general than the other datasets ($0.48-0.67$). This data set is noisier than the other three data sets. The lowest medCC-EGM values in Bord-1 were observed in BL3 and BL6. For the three clean data sets (Bord-2, Utah-1, Utah-2), for the most part, no interpolation method was better than simple removal, and instead could be quite detrimental to CC in some cases (CC reduced by up to 5.4% vs 2.1% for removal). For the noisy data set (Bord-1), the results of removal were similar to interpolation. For BL3, interpolation is substantially worse than RMV (KRI, being the worst has $\sim$25% decrease in median CC compared to RMV) but for BL4, it is the opposite (KRI, being the best has $\sim$25% increase in median CC compared to RMV). For BL4, interpolation did recover important data that is lost with removal. IF has the best overall performance—

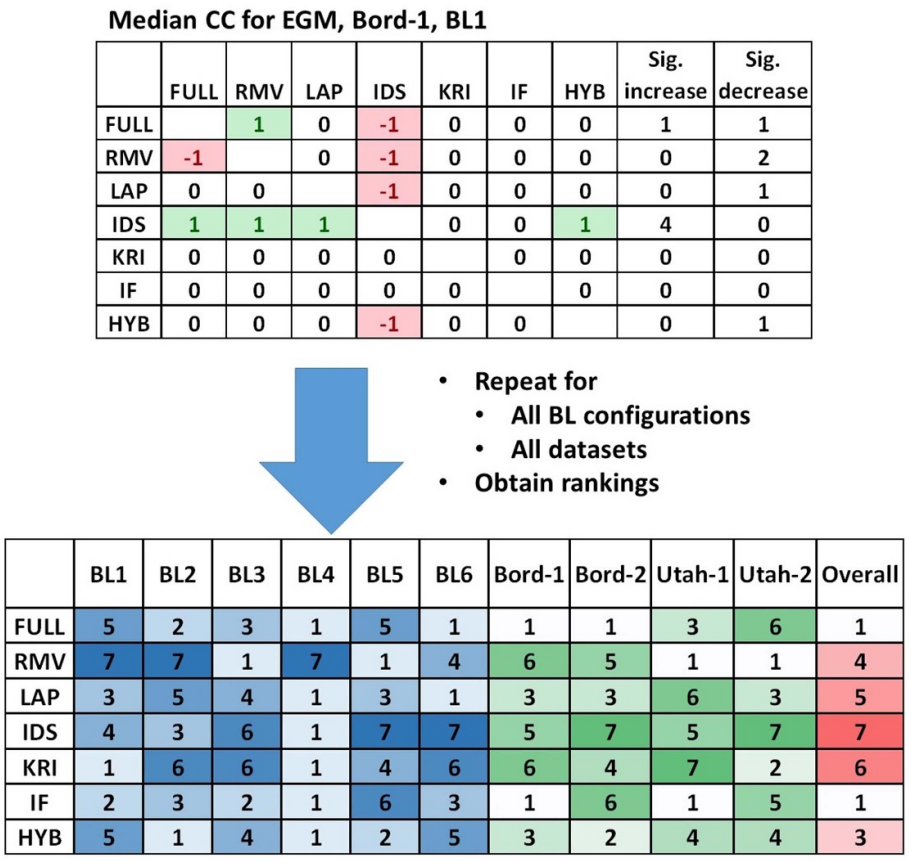

	FULL	RMV	LAP	IDS	KRI	IF	HYB	Sig. increase	Sig. decrease
FULL		1	0	-1	0	0	0	1	1
RMV	-1		0	-1	0	0	0	0	2
LAP	0	0		-1	0	0	0	0	1
IDS	1	1	1		0	0	1	4	0
KRI	0	0	0	0		0	0	0	0
IF	0	0	0	0	0		0	0	0
HYB	0	0	0	-1	0	0		0	1

	BL1	BL2	BL3	BL4	BL5	BL6	Bord-1	Bord-2	Utah-1	Utah-2	Overall
FULL	5	2	3	1	5	1	1	1	3	6	1
RMV	7	7	1	7	1	4	6	5	1	1	4
LAP	3	5	4	1	3	1	3	3	6	3	5
IDS	4	3	6	1	7	7	5	7	5	7	7
KRI	1	6	6	1	4	6	6	4	7	2	6
IF	2	3	2	1	6	3	1	6	1	5	1
HYB	5	1	4	1	2	5	3	2	4	4	3

Figure 3. Illustration of ranking steps for comparing different interpolation methods for reconstructing the EGMs. The layout of this figure is similar to that in figure 2; the metric displayed is the median temporal CC of the reconstructed EGMs. Top panel again corresponds to Bord-1, BL1. FULL and RMV are also included in this comparison.

similar to FULL. The BL6 configuration resulted in substantially reduced accuracy for the Bordeaux data sets, but not for the Utah data sets.

Despite these high medCC-EGM values, we observed poorer performance in almost all reconstructions based on the medRE-EGM metric, with a range of $0.73-0.93$. Again, the Bord-1 dataset had the worst performance ($0.85-0.93$) and the two Utah datasets had the best reconstructions ($0.73-0.79$ and $0.76-0.79$ for Utah-1 and Utah-2, respectively).

The high MedCC-EGM values indicate a good fidelity of the reconstruction morphologies to the ground truth, but poor performances in terms of the MedRE-EGM values indicate that the amplitudes in the reconstructions were not well-preserved. Thus, we took a more careful look at some individual reconstruction performances below.

Figures 4 and 5 show in panel (A) the temporal CC distributions over the heart surfaces from two different views (top and bottom) for Bord-1 and Utah-1, respectively, for a sample beat. Here, we selected the noisiest (Bord-1) and a clean (Utah-1) data set to evaluate the performances under varying noise conditions. In panel (B), sock recordings (top row) and reconstructed EGMs (bottom row) are given for 5 leads, marked on the heart surfaces. BL6 is chosen here to demonstrate the performance for the worst-case scenario.

In Bord-1 (figure 4), top row shows a negative CC region near the base that is present in all reconstructions. This region covered a smaller area for the interpolation methods compared to FULL and RMV. The negative region near the apex (slightly below point 2) was seen only in LAP, IDS, and KRI but not in FULL, RMV, IF, and HYB. Bottom row shows a large negative CC region, which covers a larger area in FULL and RMV compared to the interpolation methods.

Illustrative nodes were selected from well-reconstructed (leads 2 and 5, high-CC) and badly-reconstructed (leads 1, 3, and 4, low-CC) regions. In 2 and 5, the morphology of the reconstructed beats highly matches that of the ground truth. However, different methods yield varying amplitudes, all of which are lower than the ground truth peak-to-peak amplitude. The ground truth sock EGMs have anomalous morphologies due to drug interventions, which makes it hard to assess the performance of the ECGI reconstructions in 1, 3 and 4, and which could be one of the reasons why ECGI performed poorly in

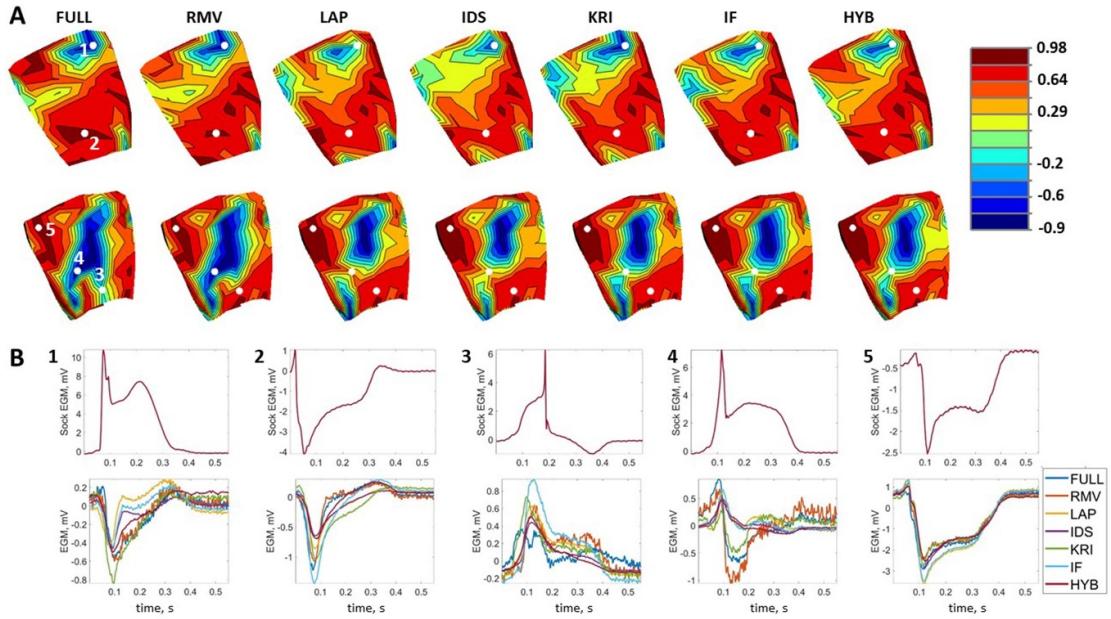

Figure 4. Sample evaluation results for Bord-1, BL6. (A) Temporal CC maps over the sock surface from two different views (top and bottom). (B) Sock (top row) and reconstructed EGMs from five different nodes (marked on the CC maps) for all methods (bottom row).

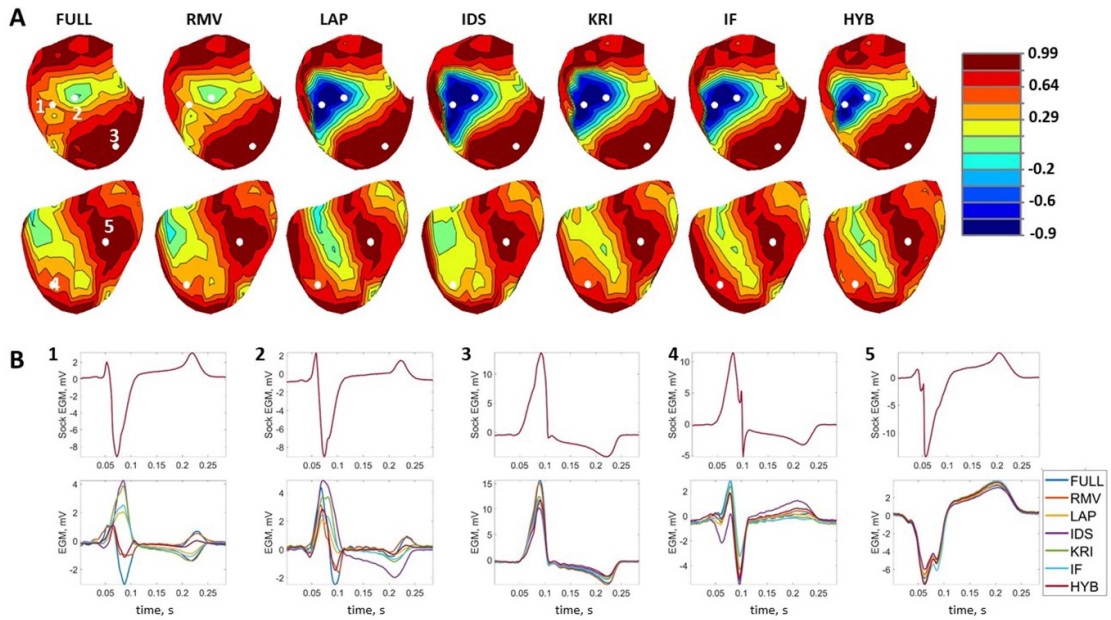

Figure 5. Sample evaluation results for Utah-1, BL6. Same format as the previous figure (A) Temporal CC maps over the sock surface from two different views (top and bottom). (B) Sock and reconstructed EGMs from five different nodes (marked on the CC maps) for all methods.

this data set. Still, one can observe that the peak-to-peak amplitudes of various reconstructions differ in general.

In Utah-1 (figure 5), top row shows a negative CC region that is present in all interpolation-based reconstructions. This region covered a smaller area for HYB compared to the other interpolation methods. FULL and RMV also had a similarly badly reconstructed (low-CC) region but not as detrimental as in the interpolation methods. The bottom row shows a low-CC region, similar in shape for all methods, but slightly smaller in size in KRI, IF, and HYB.

Again, illustrative nodes were selected from well-reconstructed (leads 3 and 5, high-CC) and badly-reconstructed (leads 1, 2, and 4, low-CC) regions. In 3, other than a variation in the reconstructed EGM amplitudes, all signal morphologies had high-fidelity to sock recordings. In 5, all reconstructions had

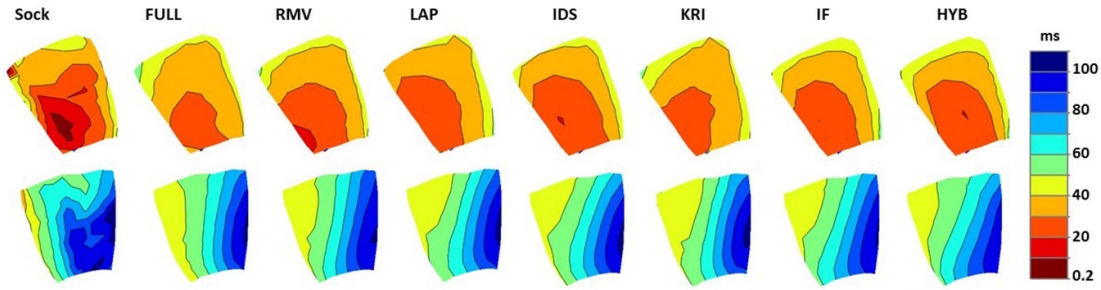

Figure 6. AT maps for a sample beat for Bord-1, BL6.

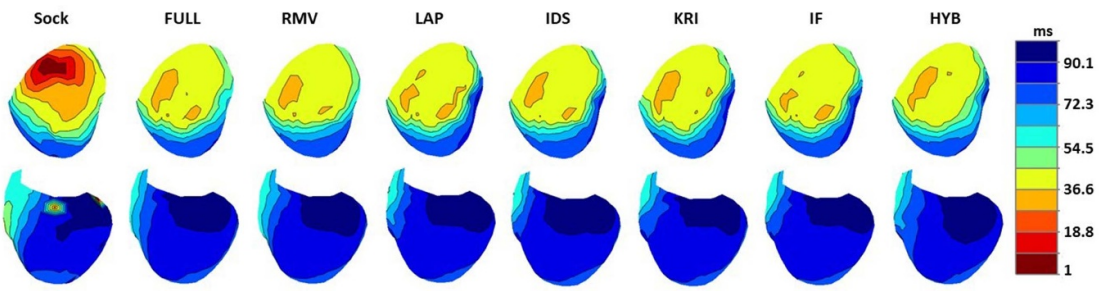

Figure 7. AT maps for a sample beat for Utah-1, BL6.

similar morphology, which matches the sock potential on average. However, the reconstructed EGMs had a larger notch than was observed in the recorded EGM. In 1, all reconstructions differ from the sock beat in amplitude and morphology; there is a reversal of polarity in the reconstructed EGMs, especially in LAP IDS, KRI, and IF. FULL, RMV, and HYB retained the biphasic morphology of the ground truth to some extent.

3.2.2. AT estimation performance

The AT estimates of the reconstructed EGMs with both ST methods gave similar AT and LE metrics, therefore, in the first part of this section, we only present results using the ST smoothing method of Erem *et al* (2014). The differences in these methods are illustrated later in figures 8 and 9, and assessed in the corresponding text.

In both Bordeaux data sets and in Utah-1, estimated AT maps represent the ground truth AT distributions accurately for all inverse reconstructions. In Bord-1, almost all of the median CC-AT values are greater than 0.90, except for LAP and HYB in BL3 (0.84) and RMV in BL4 (0.81). In Bord-2, except IDS in BL6, all median CC-AT are also over 0.90. In Utah-1, the values range between $0.86-0.92$. Utah-2 range falls to $0.75-0.79$, mostly due to a shift in the early AT estimates to later time instances. Median MAE-AT values for all reconstructions range between $4.3-8.9$ ms in Bord-2 and both Utah data sets. The errors in the exact timing of activation gets worse in Bord-1, with a range of $13.0-24.0$ ms.

Figures 6 and 7 show the ground truth and estimated AT distributions over the heart surfaces from two different views (top and bottom) for Bord-1 and Utah-1, respectively, for a sample beat in the BL6 configuration. Usually differentiating one method from another was difficult visually. The ST method inherently applies spatial smoothing on the AT maps, therefore some fine details and variations cannot be observed with the AT maps. Reconstructed EGM AT estimations in figure 7 had better fidelity to the ground truth AT distributions at late-activated regions (bottom view). However, early activated regions were not represented correctly; despite a general fit to the ground truth maps, earliest ATs were estimated with a delay.

Figures 8 and 9 illustrate the beat-to-beat variation in AT estimates of representative sock leads for Bord-1 and Utah-1, respectively. In these plots, panels A-D show EGMs and the corresponding AT estimates for four different leads. In each panel, the top row shows the average ground truth sock EGM, with the median sock AT (over all beats) marked with a red line. The bottom rows show all beats for the reconstructed EGMs (FULL reconstruction shown) and the corresponding AT estimates with three different AT estimation methods; red lines stand for the temporal $\min(\mathrm{d}V/\mathrm{d}T)$ approach, blue lines represent ST method (Erem *et al* 2014) that is also used in our evaluations, magenta lines belong to the SC method proposed in Duchateau

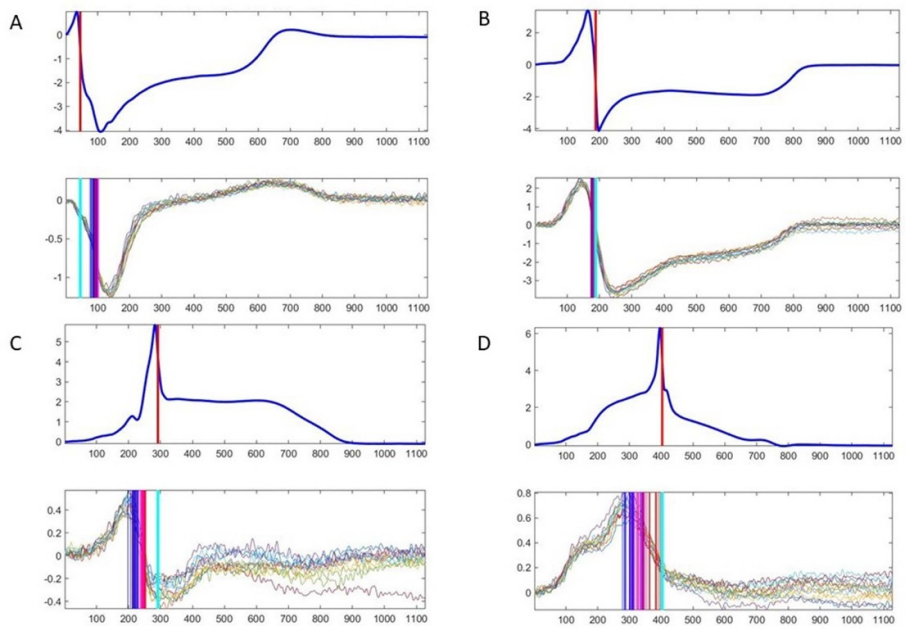

Figure 8. Panels A-D: EGMs and the corresponding AT estimates for four different leads for Bord-1. For each panel, the top row shows the average ground truth sock EGM, with the median sock AT (over all beats) marked with a red line. The bottom rows show all beats for the FULL EGM reconstruction and the corresponding AT estimates, red-temporal AT (mindVdT), blue-spatiotemporal (ST), magenta-spatially coherent (SC), cyan-median sock AT.

et al (2017), and cyan lines are the ground truth median sock AT. Note that despite pre-filtering, Bord-1 is still extremely noisy, hence the reconstructed EGMs are also noisy. Utah-1 is a clean (high SNR) dataset.

Bord-1 leads that were reconstructed with less beat-to-beat variability and noise have quite stable AT reconstructions with all three methods (figure 8, panels (A) and (B)). Furthermore, these AT reconstructions had good fidelity to the ground truth. In panel (A), due to temporally smooth EGM reconstruction, ATs were estimated later than the ground truth AT. When the reconstructed EGMs are noisy (figure 8, panels (C) and (D)), there is large beat-to-beat variability of the AT estimates, which explains higher MAE-AT values with this data set. In Utah-1 (figure 9), panels (A) and (B) had good reconstructions. In panel (C), the ground truth had early AT, but the reconstructed EGM found the AT at a later time; although the AT estimate was good considering the reconstructed EGMs, it was late with respect to the ground truth AT. The example in panel (D) shows a fragmented EGM reconstruction, which in turn affects the correct timing of the AT estimates.

3.3. Summary of statistical tests

3.3.1. Interpolated ECG leads

Combined ranking tables as shown in figure 2 were constructed for the median temporal CC (medCC-ECG) and median temporal RE (medRE-ECG) metrics of the interpolated ECG leads. Figure 10 presents the summary of these rankings. In the top panel, overall rankings for each metric are summarized. In the bottom panel, detailed overall rankings are given combining all metric performances. Detailed rankings are available in the supplementary file.

BL1 to BL6 rankings: HYB had the highest ranking for all BL configurations, and IDS was consistently the worst. IF and KRI were the next two best methods, having the second and third rankings except in BL4, in which IF ranked fourth after HYB, LAP, and KRI. In BL3, KRI shared the 1st ranking with HYB. LAP took the 4th place for all BL configurations except for BL4.

Datasets: HYB ranked the first, except in Bord-1 for which it had the third place after IF and KRI. IDS again ranked the worst. KRI ranked second except in Utah-2. IF rankings ranged from 1 to 4. LAP had the third and fourth-best scores for the Bordeaux and Utah datasets, respectively.

Overall performance based on all datasets, BL configurations, and all ECG metrics: HYB performed the best, IDS the worst, and KRI, IF, and LAP ranked second to fourth.

Individual metrics: MedCC and MedRE overall ranks were both the same as the above-mentioned overall performance.

Note that with the exception of IDS in a few cases and LAP in one case (see section 3.1), median CC values are above 0.98 but the median RE values show more variation among the methods. For most of the

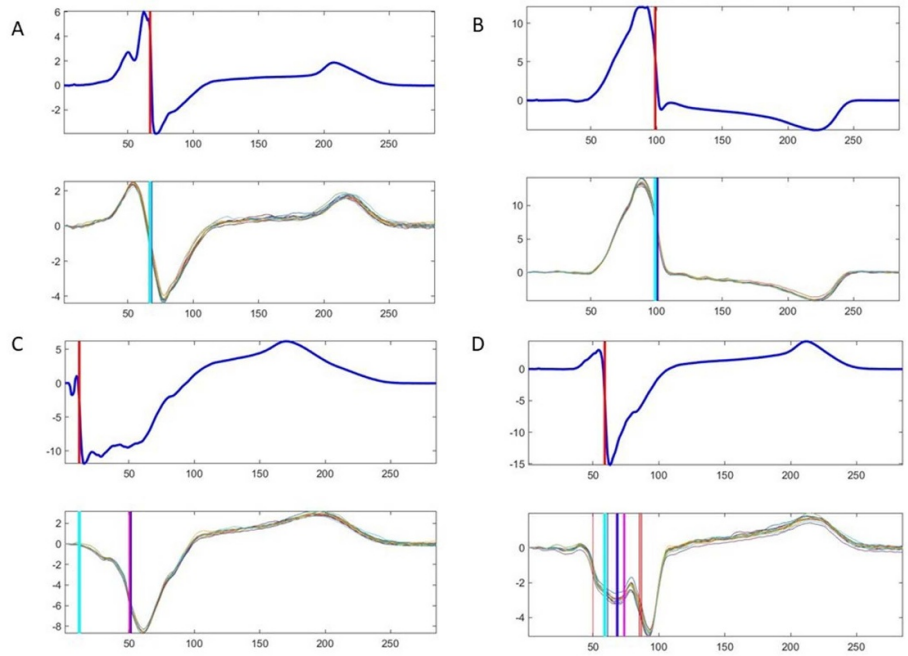

Figure 9. Panels A-D: EGMs and the corresponding AT estimates for four different leads for Utah-1. The description of plots is the same as in figure 12.

Combined ECG rankings of each metric

	MedCC-ECG	MedRE-ECG	Overall ECG
LAP	4	4	4
IDS	5	5	5
KRI	2	2	2
IF	3	3	3
HYB	1	1	1

Combined ECG rankings

	BL1	BL2	BL3	BL4	BL5	BL6	Bord-1	Bord-2	Utah-1	Utah-2	Overall
LAP	4	4	4	2	4	4	3	3	4	4	4
IDS	5	5	5	5	5	5	5	5	5	5	5
KRI	3	2	1	3	2	3	2	2	2	3	2
IF	2	2	3	4	3	2	1	4	3	2	3
HYB	1	1	1	1	1	1	3	1	1	1	1

Figure 10. Combined overall ECG rankings in terms of individual metrics (left) and with respect to different BL configurations and data sets (right).

cases IF performance is similar to HYB or KRI performance, but higher median RE values of IF attained in Bord-2, BL3 (0.45) and Utah-1, BL4 (0.32) ranks this method worse than the other two. Detailed rankings are available in the supplementary file.

3.3.2. ECGI performance

Figure 11 shows the combined ranking tables for all ECGI and AT evaluation metrics. Metrics included in these comparisons are median temporal CC (medCC-EGM), mean temporal CC (meanCC-EGM), median temporal RE (medRE-EGM), median spatial CC (medspatCC-EGM), CC of ATs (CC-AT), MAE in AT values (MAE-AT), and LE. As in figure 10, the top panel shows the overall rankings for each metric, and the bottom panel displays the detailed overall rankings. Detailed rankings are available in the supplementary file.

Overall performance based on all datasets, BL configurations, and all ECGI metrics: Overall performances of all ECGI metrics based on the ranking of different approaches varied among BL configurations and datasets. When all rankings were combined, FULL had the best performance and IDS had the worst. RMV ranked fourth with HYB (2nd) and IF (3rd) outranking LAP and KRI (both 5th) were worse than RMV.

Individual metrics: FULL had the best performance for all metrics except MAE-AT (ranks third). RMV had the worst performance of all methods in terms of MAE-AT. Considering the ECGI metrics other than MAE-AT:

IF was better than RMV based on MedCC and CC-AT, similar to RMV based on MeanCC and MedRE, and worse than RMV based on MedspatCC. It ranked first along with FULL based on MedCC. These results would suggest that IF improves the global pattern of activation and exact timing compared to RMV but is worse in terms of the exact timing of activation compared to most interpolation methods. This could impact

Combined ECGI rankings of each metric

	MedCC-EGM	MeanCC-EGM	MedRE-EGM	Med spatCC-EGM	CC-AT	MAE-AT	LE	Overall ECGI
FULL	1	1	1	1	1	3	1	1
RMV	4	3	4	2	3	7	3	4
LAP	5	3	6	7	5	1	3	5
IDS	7	6	7	4	6	6	3	7
KRI	6	6	3	4	7	3	1	5
IF	1	3	4	6	2	5	3	3
HYB	3	1	2	3	3	1	3	2

Combined ECGI rankings

	BL1	BL2	BL3	BL4	BL5	BL6	Bord-1	Bord-2	Utah-1	Utah-2	Overall
FULL	5	2	1	2	5	1	5	1	1	3	1
RMV	7	5	2	7	2	5	7	5	2	4	4
LAP	1	4	5	4	1	3	4	3	6	1	5
IDS	5	3	5	1	7	7	2	7	7	5	7
KRI	4	5	7	4	4	6	6	4	5	5	5
IF	2	7	3	6	6	4	1	5	4	2	3
HYB	3	1	4	3	3	2	3	2	3	5	2

Figure 11. Combined overall ECGI and AT rankings in terms of individual metrics (left) and with respect to different BL configurations and data sets (right).

cardiac velocity estimation. It has the second worst ranking in terms of MedspatCC after LAP, despite its best performance in terms of MedCC. This result would imply that despite better fidelity to the sock EGMs in each lead, potential maps at each time instant deviate from the true maps, possibly due to shifts in the correct position of the wavefront over the heart surface. This would also explain its poor performance in terms of MAE-AT. Its performance in terms of LE, on the other hand, is as good as the other methods (ranking after KRI).

KRI was worse than RMV for all metrics except in MedRE and LE. Despite its lower ranking in terms of CC-AT compared to other interpolation methods, it is still among the best in terms of MAE-AT. This is the opposite of what we observed with IF; KRI is better than most methods in terms of capturing the exact timing of activation. It is the best ranking method along with FULL in terms of LE, implying that it maintains accuracy for localizing PVCs.

HYB was better than RMV based on MedCC, MeanCC, and MedRE, similar to RMV based on CC-AT, and worse than RMV based on MedspatCC. It ranked first along with FULL based on MeanCC. Still, it is among the best three methods including FULL and RMV in all metrics.

LAP was worse than RMV for all metrics except in MeanCC, for which both ranked the same. Along with HYB, it is the best ranking method in terms of MAE-AT, thus capturing the exact timing of activation better than the other methods.

IDS was worse than RMV for all metrics, and most of the time performed worse than all other interpolation methods.

3.4. Relationship between ECG interpolation and ECGI performances

Figures 12 and 13 show the RMS value distributions over the torso (panel (B)), AT (panel (C)) and the temporal CC (panel (E)) distributions over the heart surfaces for BL6 configuration (panel (A)). The position of the heart with respect to the torso is also provided for reference (panel (D)). In Bord-1 (figure 12), the best ECG interpolation performances based on the temporal RE metric were by IF and HYB, closely followed by KRI, and then LAP, with IDS coming last. Qualitatively, one can observe this performance on the RMS plots of panel (B). Based on the temporal CC metric, the rankings from best to worst were by IF, closely followed by HYB and LAP, with KRI and IDS sharing the last place. On visual inspection of the maps, the worst and best performances of the methods can be observed, but despite these variations in the ranks, it is not easy to differentiate the mid-ranking methods. In the AT reconstructions, IF was again the best in terms of CC, but in this case, KRI had the lowest performance, with IDS 2nd, LAP, and HYB sharing the 3nd rank. However, these differences were minor and were not clearly visible on visual inspection of the AT maps in panel (C) (median CC-AT range is $0.92 - 0.94$). Rankings of the AT performance based on MAE, however were different; KRI and HYB shared the 1st place, and IF ranked the last, LAP and IDS in between. Still, the median MAE ranged between $14 - 16$ ms, thus it is hard to strongly suggest that one method was better than the others. In this example, AT reconstruction in the RMV was worse than the interpolation methods, as observed in the maps of panel (C).

In Utah-1 (figure 13) the rankings from best to worst based on the temporal RE metric were by HYB, KRI, IF, LAP, and finally IDS. Visual inspection of the RMS plots of panel (B) shows slight differences between the HYB, KRI, and IF maps, while LAP and IDS maps display poor ECG interpolation performance. In the temporal CC maps of panel (E), HYB clearly shows superior performance than the other interpolation methods, coming next after RMV and FULL in accuracy. HYB is followed by IF and LAP, then by KRI, and finally IDS (worst). In the AT reconstructions, HYB was again the best in terms of CC, followed by all other interpolation methods. However, there was a small variation between the median CC values ($0.86 - 0.87$). Rankings of the AT performance based on MAE were again different; this time HYB came after the other methods with a very small difference in the median MAE values ($\sim$0.5 ms).

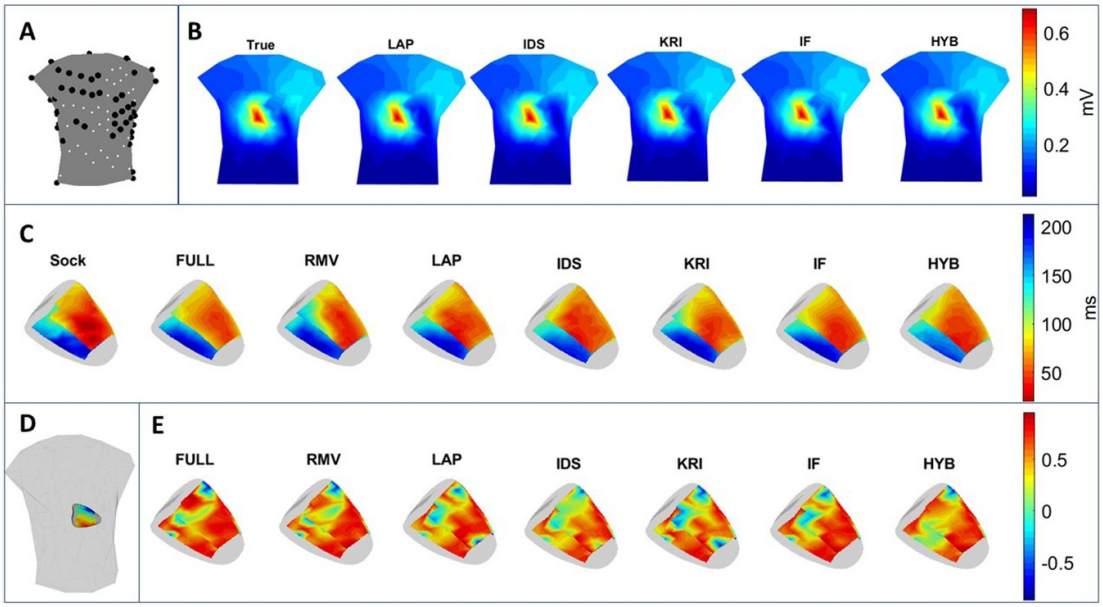

Figure 12. Sample maps for Bord-1, BL6. (A) BL6 configuration, frontal view. (B) RMS value distribution over the torso for the ground truth and the interpolated ECGs. Only the missing leads show the interpolated RMS value, the measured leads have the ground truth RMS. (C) AT isochrone maps. (D) Position of the heart with respect to the torso. (E) Temporal CC distribution over the sock.

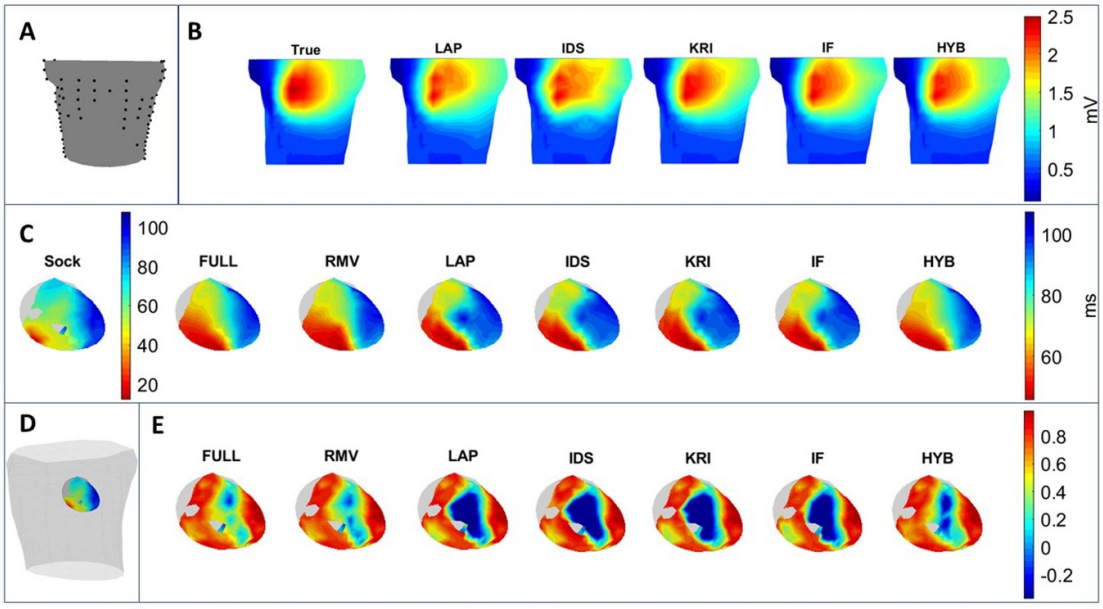

Figure 13. Sample maps for Utah-1, BL6. Panel descriptions are the same as in figure 12.

3.4.1. Summary of statistical tests

The relationship between overall ECG reconstruction performance and overall ECGI performance of all interpolation methods was presented in figure 14. Here, the summary of statistical tests in sections 3.3.1 and 3.3.2 are combined. Since ECG reconstructions do not have a corresponding performance, FULL and RMV rankings were removed from the overall ECGI performance and only the interpolation methods were ranked among themselves. HYB ranked the first and IDS ranked the last for both reconstructions. Overall IF, KRI, and LAP performances were different for each reconstruction:

- KRI ranked second for ECG reconstruction but came the 4th for ECGI.
- Although IF ranked third in terms of ECG reconstructions, it was the second best for ECGI.
- LAP ranked the 4th in terms of ECG reconstructions but it had the 3rd rank for ECGI.

	ECG	ECGI
LAP	4	3
IDS	5	5
KRI	2	3
IF	3	2
HYB	1	1

Figure 14. Relationship between overall ECG reconstruction and ECGI performances of all interpolation methods.

4. Discussion

In this study, we explored how interpolating or removing BLs affects EGM reconstructions in ECGI. We used four different experimental data from two centers. Six BL configurations were designed based on clinical experience. The more common scenario where only one or two leads present abnormal data is not addressed in this study, since the surrounding good leads provide sufficient information due to the spatial correlation and redundancy in the lead system (Ghodrati *et al* 2007, Gharbalchi No *et al* 2020). This means that while interpolation accuracy will be high, removing the single electrode will also have little to no impact on the inverse solution and the computational cost required to interpolate these signals would probably not be worthwhile. The removal of these few leads would be preferable to including those BLs in the inverse calculation. BL6 configuration was included in this study to mimic extreme conditions in the EP laboratory where both CARTO and defibrillation electrodes are attached to the patients and some leads have poor signal quality. As such, we were able to determine the viability of using these limited data sets for ECGI in combination with interpolation or BL removal.

EGMs were reconstructed using the complete (full) data, BLs-removed data, and interpolated data with five different interpolation methods, by applying zero-order Tikhonov regularization. Results presented in this study show that there is no single approach for handling BLs that stands out for all datasets and all BL configurations. Rather, different approaches were more successful compared to others based on the BL configuration or dataset. Performances of the methods also vary in terms of different metrics. Moreover, the removal of the BLs, even in the extreme BL6 scenario, did not significantly degrade the ECGI reconstructions.

4.1. ECG interpolation performance

All interpolation methods resulted in median temporal CC values above 0.9, and in most cases close to 1.00, which signifies good fidelity of ECG morphology to ground truth in the interpolated leads. However, we observed median temporal RE values as high as $0.6-0.7$ depending on the dataset, BL configuration, and the interpolation method choice. In IDS, RE values were significantly higher than the other methods in most cases, and HYB values were significantly lower, closely followed by IF and KRI in performance.

The summary of statistical tests presented in figure 10 also reflects that overall performance considering all metrics ranks HYB as the best, KRI as the second best, closely followed by IF, and IDS as the worst method of interpolation.

4.2. ECGI performance with interpolation or removal of BLs

When the overall statistical test evaluations of figure 11 are examined closely, it is hard to claim one interpolation method is always superior to the others. These rankings significantly depend on the dataset, BL configuration, and the metric used to evaluate the results.

Only after pooling all comparisons into a single ranking, one can say HYB has the second-best performance after using all available ECG leads (FULL), closely followed by IF. However, HYB is a two-step interpolation method, and it assumes that at least some beats with high signal quality are available from the BLs, and these beats are used for training. These leads are not always available, especially in the CARTO reference electrodes (BL3) or defibrillation patch (BL1 and BL2) scenarios.

IF had superior performance based on MedCC-EGM and CC-AT, however, it displayed worse performance in terms of MedspatCC-EGM and MAE-AT. This suggests that IF improves the global pattern of activation, but is worse in terms of exact timing of activation compared to most interpolation methods. This could impact cardiac velocity estimation with this method. Still, IF has the second-best performance in the overall evaluations after HYB, thus, it could be a better alternative in cases where HYB is not applicable. KRI was better than most methods in terms of capturing the exact timing of activation, and it was the best ranking method along with FULL in terms of LE, suggesting that it could be used for localizing PVCs.

LAP was worse than RMV for all metrics except in MeanCC, and worse than the other interpolation methods except in MAE-AT. Thus, if interpolation has to be applied, HYB, IF, or KRI would be preferable to

LAP. IDS is a simple method, which can be implemented easily based on the distances between a BL and the available leads. However, its ECGI reconstruction performance was worse than other interpolation methods and RMV. It was only successful for Bord-1 data, considering all metrics and BL configurations (ranks the second after IF), and for BL4 configuration considering all datasets and metrics (ranks the first). Thus, despite its simplicity, this method would not be the best choice for interpolation of BLs.

Removal of BLs ranks the fourth best method based on the overall evaluation. However, looking at overall evaluations based on a single metric, RMV also performs as well as the best ranking interpolation methods (see MeanCC-EGM, MedspatCC-EGM, CC-AT).

4.3. AT and LE

Temporal-only approach mindVdT for finding the AT is very sensitive to noise in the EGM reconstructions (Cluitmans *et al* 2017). Preprocessing is important; a trade-off is required so that there is no over-smoothing of the signals prior to derivative computation, while sufficient filtering is applied to avoid assigning a noise-related minimum derivative as the AT. Spatio-temporal methods proposed (Erem *et al* 2014, Duchateau *et al* 2017) and evaluated in recent studies (Cluitmans *et al* 2017, Schuler *et al* 2022) remedy this noise sensitivity to some extent. Here we adopted the spatio-temporal approach proposed by (Erem *et al* 2014), but results with the SC method (Duchateau *et al* 2017) were not different in terms of performance (figures 8 and 9).

The ST AT methods regulate the AT distributions, but over-smoothing of these AT distributions may result in missing sharp changes in the wavefront and detecting the slow/fast conducting regions. Here, we observed similar AT distributions with different approaches due to this spatial smoothing. Having fragmented beats as shown in figure 9(Utah-1, panel (D) example) affects the temporal-only selection of the correct AT. The spatio-temporal methods are not always successful in fixing this problem.

Median LE values range between 0 and 44 mm. Considering all datasets and BL configurations, KRI ranks first along with FULL, suggesting that it could be preferred as the interpolation method if the ECGI aim is PVC localization. There is no difference between the performances of the remaining methods (including RMV). This result is expected because the spatio-temporal AT estimation method smooths the AT maps.

4.4. Relationship between ECG/ECGI interpolation performance

Statistical test summary gives similar performance of ECG and ECGI rankings for the interpolation methods (figure 14), especially in the best/worst performing methods.

According to figures 12 and 13, the best and the worst ECG interpolation performances were achieved by HYB and IDS, respectively. Temporal CC plots illustrating the corresponding ECGI performances were mostly in agreement with those observations.

Overall, Bord-1 was much noisier than the other datasets, negatively impacting its ECGI performance with all methods. Other than that, there was no noticeable pattern in the performances of the interpolation methods that can be linked to a specific dataset. However, the locations of the missing leads were more significant in the ECGI performance. BL1, BL2, BL3, and BL6 removed electrodes in areas of higher potential gradient during the QRS, possibly removing the most information, significantly influencing which interpolation method could recover the signals most effectively. The results indicate that inaccurate interpolation at these leads deteriorates the ECGI performance (as indicated in the IDS results). The ECGI performance of RMV is superior to IDS, indicating that even removal of several leads is preferable to interpolating them incorrectly.

ECG morphologies are in general well-preserved by interpolation, but the amplitudes are not, as discussed previously. Variable performances with different interpolation methods indicate that accurate reconstruction of the ECG amplitudes is quite important for ECGI success. Thus, if interpolation is the preferred method for dealing with the missing/bad electrodes, this should be taken into account in choosing a method.

4.5. Limitations and future work

Despite the comprehensive evaluations presented in this study, there are still some limitations inherent in the study.

The first limitation is the method used for solving the inverse solution. Here we chose the zero-order Tikhonov regularization due to its widespread use in the ECGI applications by major research centers (Sapp *et al* 2012, Cluitmans *et al* 2017, Wang *et al* 2018, Bear *et al* 2019, Duchateau *et al* 2019, Molero *et al* 2023) rather than focusing on the 'best' inverse method to use in ECGI. This choice enhances the relevance and applicability of our findings to clinical settings, where standardized methods are crucial for consistency and reliability. However, the method's effectiveness depends on various factors such as the method used for the

forward matrix computation, the chosen constraint (zero, first, second order), or the regularization parameter and how it is defined, as extensively evaluated by Karoui *et al* (2018).

There is recent and growing interest in applying data-driven and machine-learning techniques to ECGI with better accuracy (Cámara-Vázquez *et al* 2021, Doste *et al* 2022, Onak *et al* 2022, Jiang *et al* 2023, Pilia *et al* 2023). However, these methods also have limitations in clinical applications, especially the lack of sufficient training data. We are currently exploring new methods to refine the accuracy and robustness of ECGI, ultimately improving its clinical utility in diagnosing and treating cardiac conditions.

The measurement artifacts and geometrical errors can cause the minimum derivative-based AT estimation to be inaccurate for some nodes. The ST approaches proposed in Erem *et al* (2014), Duchateau *et al* (2017)improved the AT estimates to some extent. However, there are still incorrectly marked ATs as illustrated in figures 8 and 13. Thus, there is still a need for a more robust AT estimation method to improve pacing site localization performance.

Finally, the methods proposed in this study were evaluated only by using single-site (RV) paced data, which mimics PVCs. Previous work on the optimization of reduced lead sets based on their ability to maximize diagnostic information demonstrated the variability in the number and locations of these optimum leads (Kornreich *et al* 1985, 1988, Finlay *et al* 2005, 2006, 2008a, 2008b, Guillem *et al* 2008). While we expect the general conclusions of this study to apply to a wider variety of data including sinus rhythm or different types of arrhythmias, more evaluations have to be carried out to recommend a specific method for handling missing/BLs in the clinical applications of ECGI.

5. Conclusion

This study demonstrated for the first time that removing the missing/BLs from the ECGI analysis performs comparable results with utilizing all leads. Thus, the removal of BLs would be a safer approach if one is not confident with the interpolation performance, the BLs are located at high-amplitude/high-potential gradient regions, or there are a significant number of missing leads.

Interpolation methods such as the IF or the Kriging method, which successfully take into account the spatial information and correlations of the remaining BSP leads and do not require training, often result in more accurate and reliable estimations compared to simpler interpolation methods.

These take-home messages of the study constitute a significant step towards improving the clinical utility of ECGI in diagnosing and treating cardiac conditions, especially in real-time clinical applications.

Data availability statement

The data that support the findings of this study will be openly available following an embargo at the following URL/DOI: www.ecg-imaging.org/edgar-database. Data will be available from 01 June 2025.

Acknowledgments

The authors are grateful for the support of the Consortium for ECG Imaging (www.ecg-imaging.org/). This work was supported by the French National Research Agency (ANR-10-IAHU04-LIRYC); by Maastricht University Medical Center and Hasselt University (BOF17DOCMA15); by the research Grant 2/0109/22 from the VEGA Grant Agency in Slovakia and APVV-19-0531 from the Slovak Research and Development Agency.

ORCID iDs

Y Serinagaoglu Dogrusoz https://orcid.org/0000-0002-5926-644X
L R Bear https://orcid.org/0000-0002-7070-2492
J A Bergquist https://orcid.org/0000-0002-4586-6911
A S Rababah https://orcid.org/0000-0002-2078-635X
W Good https://orcid.org/0000-0002-0111-9076
J Stoks https://orcid.org/0000-0001-8881-5498
J Svehlikova https://orcid.org/0000-0002-8932-3361
E van Dam https://orcid.org/0000-0003-1653-7323
D H Brooks https://orcid.org/0000-0003-3231-6715
R S MacLeod https://orcid.org/0000-0002-0000-0356

References

Barr R C, Ramsey M and Spach M S 1977 Relating epicardial to body surface potential distributions by means of transfer coefficients based on geometry measurements *IEEE Trans. Biomed. Eng.* **BME-24** 1–11

Barr R C, Spach M S and Herman-Giddens G S 1971 Selection of the number and positions of measuring locations for electrocardiography *IEEE Trans. Biomed. Eng.* **BME-18** 125–38

Bear L R *et al* 2019 Advantages and pitfalls of noninvasive electrocardiographic imaging *J. Electrocardiol.* **57** S15–S20

Bear L R *et al* 2021 The impact of torso signal processing on noninvasive electrocardiographic imaging reconstructions *IEEE Trans. Biomed. Eng.* **68** 436–47

Bear L R, Huntjens P R, Walton R D, Bernus O, Coronel R and Dubois R 2018 Cardiac electrical dyssynchrony is accurately detected by noninvasive electrocardiographic imaging *Heart Rhythm* **15** 1058–69

Bear L *et al* 2015 Accuracy of lead removal vs linear interpolation in non-invasive electrocardiographic imaging (ECGI) *2015 Computing in Cardiology Conf. (CinC)* (*Nice, France*) pp 941–4

Bergquist J A, Good W W, Zenger B, Tate J D and MacLeod R S 2019 GRÖMeR: a pipeline for geodesic refinement of mesh registration *Funct. Imaging Model Heart* **11504** 37–45

Bergquist J A, Good W W, Zenger B, Tate J D, Rupp L C and MacLeod R S 2021 The electrocardiographic forward problem: a benchmark study *Comput. Biol. Med.* **134** 104476

Burnes J E Kaelber D C, Taccardi B, Lux R L, Ershler P R and Rudy Y 1998 A field-compatible method for interpolating biopotentials *Ann. Biomed. Eng.* **26** 37–47

Cámara-Vázquez M A, Hernández-Romero I, Morgado-Reyes E, Guillem M S, Climent A M and Barquero-Pérez O 2021 Non-invasive estimation of atrial fibrillation driver position with convolutional neural networks and body surface potentials *Front. Physiol.* **12** 733449

Castells F, Guillem M, Climent A, Bodi V, Chorro F and Millet J 2007 Performance evaluation in the reconstruction of body surface potentials from reduced lead systems a comparative study of lead selection algorithms *2007 Computers in Cardiology* (*Durham, NC, USA*) pp 713–6

Cluitmans M J M *et al* 2017 *In Vivo* validation of electrocardiographic imaging *JACC: Clin. Electrophysiol.* **3** 232–42

Cluitmans M *et al* 2018 Validation and opportunities of electrocardiographic imaging: From technical achievements to clinical applications *Front. Physiol.* **9** 1305

Cluitmans M, Peeters R Westra R and Volders P 2015 Noninvasive reconstruction of cardiac electrical activity: update on current methods, applications and challenges *Neth. Heart J.* **23** 301–11

Cressie N 1990 The origins of Kriging *Math. Geol.* **22** 239–52

Dogrusoz Y S *et al* 2019 Effects of interpolation on the inverse problem of electrocardiography *2019 Computing in Cardiology (CinC)* (*Singapore*) pp 1–4

Donnelly M P, Finlay D D, Nugent C D and Black N D 2008 Lead selection: old and new methods for locating the most electrocardiogram information *J. Electrocardiol.* **41** 257–63

Doste R, Lozano M, Jimenez-Perez G, Mont L, Berruezo A, Penela D, Camara O and Sebastian R 2022 Training machine learning models with synthetic data improves the prediction of ventricular origin in outflow tract ventricular arrhythmias *Front. Physiol.* **13** 909372

Duchateau J *et al* 2019 Performance and limitations of noninvasive cardiac activation mapping *Heart Rhythm* **16** 435–42

Duchateau J Potse M and Dubois R 2017 Spatially coherent activation maps for electrocardiographic imaging *IEEE Trans. Biomed. Eng.* **64** 1149–56

Erem B, Coll-Font J, Orellana R M, St'Ovicek P and Brooks D H 2014 Using transmural regularization and dynamic modeling for noninvasive cardiac potential imaging of endocardial pacing with imprecise thoracic geometry *IEEE Trans. Med. Imaging* **33** 726–38

Finlay D D, Nugent C D, Donnelly M P and Black N D 2008a Selection of optimal recording sites for limited lead body surface potential mapping in myocardial infarction and left ventricular hypertrophy *J. Electrocardiol.* **41** 264–71

Finlay D D, Nugent C D, Donnelly M P, Lux R L, McCullagh P J and Black N D 2006 Selection of optimal recording sites for limited lead body surface potential mapping: a sequential selection based approach *BMC Med. Inform. Decis. Making* **6** 9

Finlay D D, Nugent C D, Donnelly M P, McCullagh P J and Black N D 2008b Optimal electrocardiographic lead systems: practical scenarios in smart clothing and wearable health systems *IEEE Trans. Inform. Technol. Biomed.* **12** 433–41

Finlay D D, Nugent C D, McCullagh P J and Black N D 2005 Mining for diagnostic information in body surface potential maps: a comparison of feature selection techniques *Biomed. Eng. Online* **4** 51

Gharbalchi No F, Serinagaoglu Dogrusoz Y, Onak O and Weber G-W 2020 Reduced leadset selection and performance evaluation in the inverse problem of electrocardiography for reconstructing the ventricularly paced electrograms *J. Electrocardiol.* **60** 44–53

Ghodrati A , Brooks D H and MacLeod R S 2007 Methods of solving reduced lead systems for inverse electrocardiography *IEEE Trans. Biomed. Eng.* **54** 339–43

Guillem M S, Castells F, Climent A M, Bodí V, Chorro F J and Millet J 2008 Evaluation of lead selection methods for optimal reconstruction of body surface potentials *J. Electrocardiol.* **41** 26–34

Hansen P C 2001 The L-curve and its use in the numerical treatment of inverse problems *Computational Inverse Problems in Electrocardiography*, ed P R Johnston (WIT Press) ch 4, pp 119–42

Hoekema R Uijen G J H and van Oosterom A 1999 On selecting a body surface mapping procedure *J. Electrocardiol.* **32** 93–101

Jiang X, Toloubidokhti M, Bergquist J, Zenger B, Good W W, MacLeod R S and Wang L 2023 Improving generalization by learning geometry-dependent and physics-based reconstruction of image sequences *IEEE Trans. Med. Imaging* **42** 403–15

Karoui A, Bear L, Migerditichan P and Zemzemi N 2018 Evaluation of fifteen algorithms for the resolution of the electrocardiography imaging inverse problem using ex-vivo and in-silico data *Front. Physiol.* **9** 1708

Kornreich F, Montague T J, Rautaharju P M, Kavadias M and Horacek M B 1988 Identification of best electrocardiographic leads for diagnosing left ventricular hypertrophy by statistical analysis of body surface potential maps *Am. J. Cardiol.* **62** 1285–91

Kornreich F, Rautaharju P M, Warren J, Montague T J and Horacek B 1985 Identification of best electrocardiographic leads for diagnosing myocardial infarction by statistical analysis of body surface potential maps *Am. J. Cardiol.* **56** 852–6

Lux R L, Burgess M J, Wyatt R F, Evans A K, Vincent G M and Abildskov J 1979 Clinically practical lead systems for improved electrocardiography: comparison with precordial grids and conventional lead systems *Circulation* **59** 356–63

Lux R L, Smith C R, Wyatt R F and Abildskov J 1978 Limited lead selection for estimation of body surface potential maps in electrocardiography *IEEE Trans. Biomed. Eng.* **BME-25** 270–6

Molero R, Hernández-Romero I, Climent A M and Guillem M S 2023 Filtering strategies of electrocardiographic imaging signals for stratification of atrial fibrillation patients *Biomed. Signal Process. Control* **81** 104438

Nademanee K *et al* 2019 Mapping and ablation of ventricular fibrillation associated with early repolarization syndrome *Circulation* **140** 1477–90

Onak O N, Erenler T and Serinagaoglu Dogrusoz Y 2022 A novel data-adaptive regression framework based on multivariate adaptive regression splines for electrocardiographic imaging *IEEE Trans. Biomed. Eng.* **69** 963–74

Oostendorp T F van Oosterom A and Huiskamp G 1989 Interpolation on a triangulated 3D surface *J. Comput. Phys.* **80** 331–43

Pilia N, Schuler S, Rees M, Moik G, Potyagaylo D, Dossel O and Loewe A 2023 Non-invasive localization of the ventricular excitation origin without patient-specific geometries using deep learning *Artif. Intell. Med.* **143** 102619

Rababah A S *et al* 2018 An adaptive Laplacian based interpolation algorithm for noise reduction in body surface potential maps *2018 Computing in Cardiology Conf. (CinC)* (*Maastricht, Netherlands*) pp 1–4

Rababah A S *et al* 2019 Novel hybrid method for interpolating missing information in body surface potential maps *J. Electrocardiol.* **57** S51–S55

Rababah A *et al* 2021 The effect of interpolating low amplitude leads on the inverse reconstruction of cardiac electrical activity *Comput. Biol. Med.* **136** 104666

Rababah A *et al* 2019 Interpolating low amplitude ecg signals combined with filtering according to international standards improves inverse reconstruction of cardiac electrical activity *Functional Imaging and Modeling of the Heart* (*Lecture Notes in Computer Science*) vol 11504, ed Y Coudière, V Ozenne, E Vigmond and N Zemzemi (Springer) (https://doi.org/10.1007/978-3-030-21949-9_13)

Rodenhauser A, Good W, Zenger B, Tate J, Aras K, Burton B and MacLeod R 2018 PFEIFER: Preprocessing framework for electrograms intermittently fiducialized from experimental recordings *J. Open Source Software* **3** 472

Sapp J L Dawoud F, Clements J C and Horáček B M 2012 Inverse solution mapping of epicardial potentials: quantitative comparison with epicardial contact mapping *Circ. Arrhythm Electrophysiol.* **5** 1001–9

Schuler S *et al* 2022 Reducing line-of-block artifacts in cardiac activation maps estimated using ECG imaging: a comparison of source models and estimation methods *IEEE Trans. Biomed. Eng.* **69** 2041–52

Shepard D 1968 A two-dimensional interpolation function for irregularly-spaced data *Proc. 1968 23rd ACM National Conf.* (ACM) pp 517–24

Shome S and MacLeod R 2007 Simultaneous high-resolution electrical imaging of endocardial, epicardial and torso-tank surfaces under varying cardiac metabolic load and coronary flow *Functional Imaging and Modeling of the Heart. FIMH* (*Lecture Notes in Computer Science*) vol 4466, ed F B Sachse and G Seemann (Springer) (https://doi.org/10.1007/978-3-540-72907-5_33)

Stoks J Hermans B Boukens B, Holtackers R, Gommers S, Kaya Y, Vernooy K, Cluitmans M, Volders P and ter Bekke R 2023 High-resolution structural-functional substrate-trigger characterization: Future roadmap for catheter ablation of ventricular tachycardia *Front. Cardiovasc. Med.* **10** 1112980

Tikhonov A N and Arsenin V Y 1977 *Solutions of Ill-Posed Problems* (Halsted Press)

van Beers W C M and Kleijnen J P C 2003 Kriging for interpolation in random simulation *J. Oper. Res. Soc.* **54** 255–62

Wang L, Gharbia O A, Nazarian S and Horácek B M 2018 Non-invasive epicardial and endocardial electrocardiographic imaging for scar-related ventricular tachycardia *Europace* **20** f263–72

Wang Y and Rudy Y 2006 Application of the method of fundamental solutions to potential-based inverse electrocardiography *Ann. Biomed. Eng.* **34** 1272–88